Ceramics International 47 (2021) 21466–21475

Contents lists available at ScienceDirect

Ceramics International

journal homepage: www.elsevier.com/locate/ceramint

3D CaP porous scaffolds with grooved surface topography obtained by the sol-gel method

E. Sebastián [a,*], A. Murciano [b], R. Madrigal [b], P.N. De Aza [a], P. Velasquez [a]

[a] Instituto de Bioingeniería, Universidad Miguel Hernández, Avda. Universidad S/n, Elche, Alicante, 03202, Spain
[b] Departamento de Materiales, Óptica y Tecnología Electrónica, Universidad Miguel Hernández, Avda. Universidad S/n, Elche, Alicante, 03202, Spain

ARTICLE INFO

Keywords:
Sol–gel processes
Surfaces
Biomedical applications
Chemical etching

ABSTRACT

The influence of surface topography on cellular behaviour and its importance for the development of three-dimensional scaffolds for bone tissue engineering are a topic of growing interest. To date, the introduction of topographical patterns into the surface of 3D porous ceramic scaffolds has proven difficult, due partly to the brittle nature of ceramic materials as well as the currently available fabrication technologies. In this study, a grooved pattern was introduced into the surface of 3D multilayer porous ceramic scaffolds by the chemical etching technique. The patterned scaffolds were characterised by X-Ray Diffraction (XRD), Scanning Electron Microscopy with Energy Dispersive X-Ray Spectroscopy (SEM-EDX) and Digital Holographic Microscopy (DHM). Their bioactivity was also evaluated *in vitro* by immersion in simulated body fluid (SBF) for 12 h, 1, 7, 14 and 21 days. Scaffolds were constituted mainly with a mixture of the calcium pyrophosphate ($Ca_2O_7P_2$) and β-tricalcium phosphate ($Ca_3(PO_4)_2$) phases. The pyrophosphate on the external layer was dissolved as a result of the etching process, leaving grooves on the surface. Ridges and grooves were nano-/micrometric, with dimensions of around 900 nm–1.5 μm in width and 200 nm–300 nm in depth. Moreover, the mechanical properties and bioactive capacity of the patterned scaffolds were not affected by chemical etching, making them suitable to be used in bone tissue engineering.

1. Introduction

Tissue engineering has attracted plenty of research interest in recent years thanks to the development of more complex biomaterials. Particularly, in the bone tissue engineering field, three-dimensional (3D) calcium phosphate (CaP) porous scaffolds are a promising alternative to treating damaged bone tissue [1].

When developing these porous scaffolds, we need to consider their capacity to support new bone tissue formation in bioactivity and biocompatibility terms. This capacity is determined by the scaffolds' physicochemical parameters, including pore size and structure, chemical composition, surface topography, degradability rate and mechanical strength [2,3]. These properties determine the cell-material interaction and are, therefore, essential for the scaffolds' successful osseointegration.

Pore structure is one of the most important aspects of 3D scaffolds because it affects cell migration, attachment and spreading as well as the transport of nutrients and metabolic waste. Previous studies have revealed that having an interconnected porosity to promote cell ingrowth and support ingrown tissue vascularisation is highly desirable [4,5]. A porosity of around 80–90% and a pore diameter of at least 100 μm are required because they allow cell penetration and proper vascularisation of the new tissue [6]. Macropores (>100 μm) are required for cell migration and nutrient transport, while micropores (<10 μm) increase ion exchange, protein adsorption and mineralised tissue formation [3,5].

When designing bone substitute scaffolds, we need to consider not only the pore structure but also the effect of the surface characteristics on the cell behaviour. It has been well established that cellular behaviour depends on the physical and chemical characteristics of the materials surface, such as topography, particle size, crystallinity, and chemical composition [7,8].

Many works have focused on the effect of well-defined topographical patterns on the nano-/microscale with a range of cell types, including fibroblast [9], osteoblasts [10], epithelial cells [11] and endothelial cells [12].

In particular, topography effects on osteoblasts have been well documented, and include changes in adhesion [13], proliferation [8],

* Corresponding author.
E-mail address: eduardo.sebastian@goumh.umh.es (E. Sebastián).

https://doi.org/10.1016/j.ceramint.2021.04.158
Received 27 January 2021; Received in revised form 30 March 2021; Accepted 16 April 2021
Available online 20 April 2021

and differentiation [14–16], which influence bone formation. Understanding the role that surface topography plays in regulating cell behaviour is essential for designing osteoinductive 3D porous scaffolds.

Different types of nano- and microscale topographical patterns like pits, wells, pillars, pores, grooves and ridges, have been studied [17,18]. Of these surface patterns, ridges and grooves are very interesting because, this type of topographical patterns can be used to mimic the biophysical cues provided by the collagen fibres that form the bone extracellular matrix (ECM). *In vivo*, cells interact with the ECM, and this interaction is essential for regulating cell behaviour, which is why is important to develop new biomaterials that better resemble natural ECM features.

Many studies have been conducted using polymeric substrates to determine the effect of groove-like topography on human mesenchymal stem cells (hMSCs) and osteoblasts. According to Kirmizidis et al. [14], when cultured on grooved surfaces, osteoblasts tend to align in the direction of grooves, adhering to and spreading across the top and along the base of the grooves. Lenhert et al. [10] also concluded that when cultured on grooved topographies, osteoblasts align, elongate, and migrate in parallel to grooves. This phenomenon is known as ‘‘contact guidance’’ and has long since been observed [19]. Watari et al. [20] demonstrated that anisotropically ordered ridges and grooves can promote the osteogenic differentiation of hMSCs *in vitro*, and even in the absence of osteogenic supplements in some cases [21]. It would generally appear that grooved topography provides the most effective structural cues for regulating cell alignment, orientation, adhesion, and morphology compared to those cells cultured on smooth surfaces [17, 22].

Our ability to modify the surface topography and to produce nano-/microstructures has increased over the years thanks to the development of new fabrication technologies. Several fabrication methods have been applied to produce highly controlled, reproducible, and well-defined topographical patterns. Currently used nano-/microfabrication technologies include photolithography, electron beam lithography, colloidal lithography, electrospinning, polymer demixing, among others [4]. The main downside of these techniques is that they are able to generally introduce only structured patterns into flat surfaces, they require expensive equipment, are generally time-consuming processes and are also difficult to scale up.

Both the complexity of the aforementioned fabrication techniques and the fact that ceramic materials are more fragile than polymers or metals make introducing these topographical patterns into 3D CaP scaffolds difficult [17,23]. In an effort to overcome this problem, in this study we applied the chemical etching technique to introduce uniformly distributed ridges and grooves on the surface of 3D CaP porous scaffolds to be used in bone tissue engineering.

2. Materials and methods

2.1. Materials preparation

The calcium phosphate ceramics herein used were prepared by the sol-gel method in combination with the polymeric sponge replication method [24]. The core of the scaffolds, whose composition was $2SiO_2$–$50CaO$–$48P_2O_5$ (mol%), was prepared with 10.5 mL of $(C_2H_5)_3PO_4$ (TEP, Aldrich-Trietyl Phosphate), 0.2 mL of Si $(OC_2H_5)_4$ (TEOS, Aldrich-Tetraethyl Orthosilicate), 9.5 g of calcium carbonate ($CaCO_3$, Sigma), 5 mL of ethanol 97°, 20 mL of distilled water and 10 mL of hydrochloric acid (HCl 37%, Ensure), employed as reactants of the initial sol-gel solution.

In the initial step, all the reactants except calcium carbonate were mixed together and the solution was stirred for 30 min to allow the hydrolysis of precursors. Afterwards, calcium carbonate was added to the solution and pH was adjusted between 2 and 3 by adding HCl drop by drop. Polyurethane sponges (20 ppi, 12.7 mm diameter, 10 mm high) were submerged in the solution and dried in a furnace for 10 min at 180 °C. Several immersions were performed, adding new layers after each immersion, and removing any excess by centrifugation to avoid blocking the porous structure. Next, the sponges were sintered in a furnace (Naberthen, Lilienthal/Bremen, Germany) at 950 °C at heating rate of 19 °C/h for 50 h. This temperature was maintained for 8 h.

Finally, the core was coated with the external layers, whose composition was $50CaO$–$50P_2O_5$ (mol%), to obtain the multilayer scaffolds. A new sol-gel solution was prepared by mixing 10.8 mL of $(C_2H_5)_3PO_4$ (TEP, Aldrich-Trietyl Phosphate), 5 mL of ethanol 97°, 20 mL of distilled water, 10 mL of hydrochloric acid (HCl 37%, Ensure) and 8.32 g of calcium carbonate ($CaCO_3$, Sigma). The core was coated with the new solution for the appropriate number of times following the procedure described above. Scaffolds were sintered again at 950 °C at a heating rate of 119 °C/h for 8 h. This temperature was maintained for 3 h.

2.2. Scaffolds characterisation

The multilayer ceramic scaffolds were characterised by Scanning Electron Microscopy with Energy Dispersive X-Ray Spectroscopy (SEM-EDX) using a Hitachi S – 3500 N with INCA system by Oxford Instruments Analytical. All the samples were palladium-coated before being analysed.

The mineralogical composition of the material was determined by X-Ray Diffraction (XRD) in a Bruker- AXR D8 Advance automated diffractometer using Cu-Kα radiation (1.54056 Å). Data was collected in the Bragg-Brentano thetha-2thetha (θ/2θ) geometry between 20° and 46° (2θ) at 0.02 steps, counting 8 s per step. The X-ray tube was operated at 40 kV and 30 mA. The obtained diffractograms were analysed with the Match! 3 software (v. 3.10.2.173) by the Rietveld method and were compared with the Crystallography Open Database (COD).

Scaffolds' mechanical strength was determined by a compression test using a Simple Manual Test Stand (SVL-1000 N, IMADA). Load was manually applied to scaffolds (8.5 mm diameter, 10.0 mm high) until their structure collapsed. The results of 10 valid tests were used to calculate the ceramic scaffolds' compressive strength.

The porosity and pore size distribution of scaffolds was determined by the Mercury Porosimetry Technique (Poremaster 60 GT, Quantachrome instruments) at a pressure range between 72.9 bar and 4063.71 bar.

2.3. Surface topography patterning and characterisation

Ceramic scaffolds' surface was modified to introduce a topographic pattern in the form of ridges and grooves by a chemical etching process. An etching solution was prepared by dissolving acetic acid glacial (CH_3COOH, PanReac) in distilled water under stirring conditions to ensure complete chemical dissolution. Scaffolds were submerged in the etching solution under stirring to ensure that the whole surface was etched. Finally, scaffolds were rinsed with distilled water to remove any residual etching solution and dried at 75 °C for 1 h. Different concentrations (3%, 5%, 10%) and etching times (30 s, 60 s, 90 s, 120 s) were tested following the same described procedure. The whole process was conducted at room temperature.

The modified scaffolds were characterised by SEM-EDX and XRD. The dimensions, width and depth, of the ridges and grooves produced by the etching process were determined using a Digital Holographic Microscope (DHM-R2100, Lyncée Tec, Lausanne, Switzerland) with the Koala software. Measurements were taken with a 20× lens at wavelength of $\lambda = 684.9$ nm. This setup provided a horizontal resolution of 0.45 μm and a field area of 51.3×51.3 μm^2 with a height precision of 5 nm in the centre of the image and one of 20 nm on the edges. Holograms were analysed with the ParaView (ver. 5.8.0) and ImageJ (ver. 1.53) programmes.

2.4. Scaffolds' in vitro bioactivity

In order to evaluate the effect of chemical etching on the patterned scaffolds' *in vitro* bioactive capacity, bioactivity tests were conducted by immersion in simulated body fluid (SBF) following the procedure established by Kokubo et al. [25]. The samples in SBF were incubated at 37 °C in a water bath for 12 h, 1, 7, 14 and 21 days. After each time period, scaffolds were dried at 75 °C for 24 h and analysed by SEM-EDX. Changes in the calcium (Ca), silicon (Si) and phosphorus (P) ion concentrations were determined by Inductively Coupled Plasma Optical Emission Spectrometry (ICP-OES PerkinElmer Optima 2000™).

3. Results

3.1. Scaffolds characterisation

Fig. 1A shows the microstructure of the multilayer scaffolds' core analysed by SEM-EDX. The core presented an interconnected porosity, it was composed of hexagonal and triangular grains of Ca and P and had a Ca/P ratio of about 1.0, which is the stoichiometric value of calcium pyrophosphate ($Ca_2O_7P_2$). This type of microstructure is characteristic of materials with a high pyrophosphate content. Furthermore, the XRD analysis of the core confirmed that it was composed mainly of a calcium pyrophosphate phase (COD-96-151-7239).

Once the core was characterised, it was coated with a more bioactive composition to obtain the external layers of the multilayer ceramic scaffold. The multilayer scaffolds' surface was smooth with some hexagonal grains of calcium pyrophosphate and β-tricalcium phosphate (β-TCP) (β-$Ca_3(PO_4)_2$) (Fig. 1B). The EDX results showed that scaffolds were composed of Ca, P, and a small amount of Si. Their Ca/P ratio was 1.24. Fig. 2A shows the mineralogical composition of the multilayer scaffolds determined by XRD. According to the XRD patterns, the main constituent phases were calcium pyrophosphate (COD-96-151-7239) and β-tricalcium phosphate (COD-96-151-7239), although other minor silica phases like CaO_5Si_2 (COD-96-900-6569) were observed.

Fig. 3 depicts the scaffolds' pore size distribution measured by the Mercury Porosimetry Technique. The multilayer scaffolds had a total porosity of 36.95%, 32.34% of which corresponded to interparticle spaces (<300 μm) with a pore size between 173.6 μm and 7.01 μm. The remaining 4.60% corresponded to intraparticle spaces (<1 μm), with a pore size between 0.07 μm and 0.05 μm.

3.2. Scaffolds surface topography characterisation

The multilayer ceramic scaffolds were chemically etched to introduce a topographical pattern in the form of ridges and grooves into the scaffolds' surface. Fig. 4 shows the scaffolds' surface structure at several concentrations (3%, 5%, 10%) and etching times (30 s, 60 s, 90 s, 120 s). A 3% acetic acid concentration and a 120 s etching time gave the best results to consistently obtain a large amount of well-defined nano-/micrometric ridges and grooves that were uniformly distributed along the scaffolds' surface.

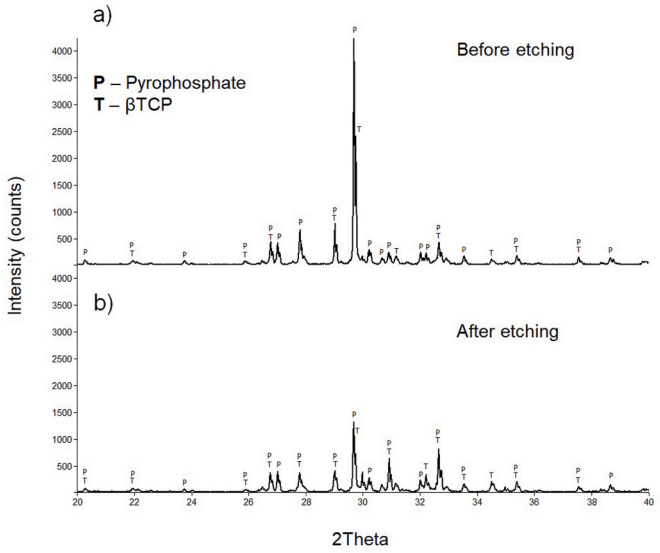

Fig. 2. XRD patterns of the multilayer scaffolds (a) before and (b) after chemical etching.

The mineralogical composition determined by XRD after etching is shown in Fig. 2B. The peaks corresponding to calcium pyrophosphate (COD-96-151-7239) and β-tricalcium phosphate (COD-96-151-7239) were slightly different compared to the diffractogram of the untreated scaffolds. The peaks corresponding to pyrophosphate were diminished, while the peaks for β-TCP were more prominent after etching. According to the EDX results, the Ca/P ratio on the surface after etching was about 1.3, with a Ca/P ratio close to 1.5 on the grooved areas.

Fig. 5 shows the three-dimensional surface profiles of the etched scaffolds analysed by Digital Holographic Microscopy (DHM) with their corresponding height profiles. High magnification SEM images were also used to determine the width of ridges (Fig. 6). The 3D surface profiles, together with the SEM images, further confirmed that ridges and grooves were uniformly distributed on scaffolds' surface. Their dimensions (width and depth) were nano-/micrometric and varied with etching time. After 60s (Fig. 5A), the ridges had a width of ~1 μm and the grooves had a depth of about 250 nm. Both ridges and grooves had similar widths. In the scaffolds etched for 120s (Fig. 5B), the width of ridges and grooves was around 850–950 μm in both cases, and the depth of grooves was of 277 nm, as seen in detail in the height profiles. Overall, their width decreased with etching time and was around 900 nm–1.5 μm, while their depth was 200–300 nm and increased with etching time.

Scaffolds' compressive strength was measured with a Manual Test Stand before and after chemical etching treatment. The untreated scaffolds' mechanical strength was 0.46–0.67 MPa, while their resistance

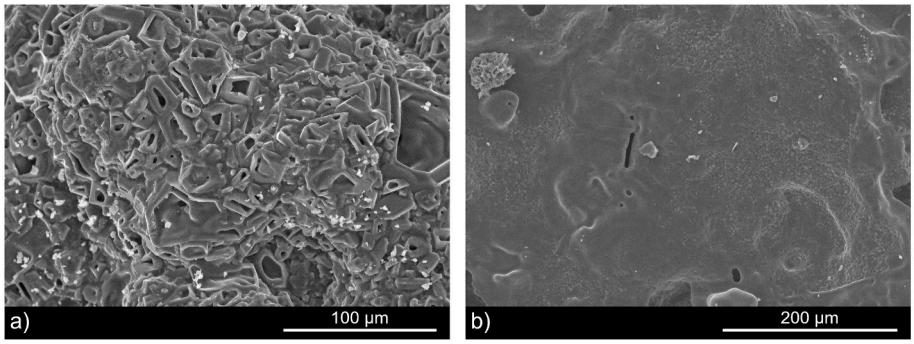

Fig. 1. SEM micrographs of the initial multilayer scaffolds microstructure: (a) core and (b) core coated with the external layers.

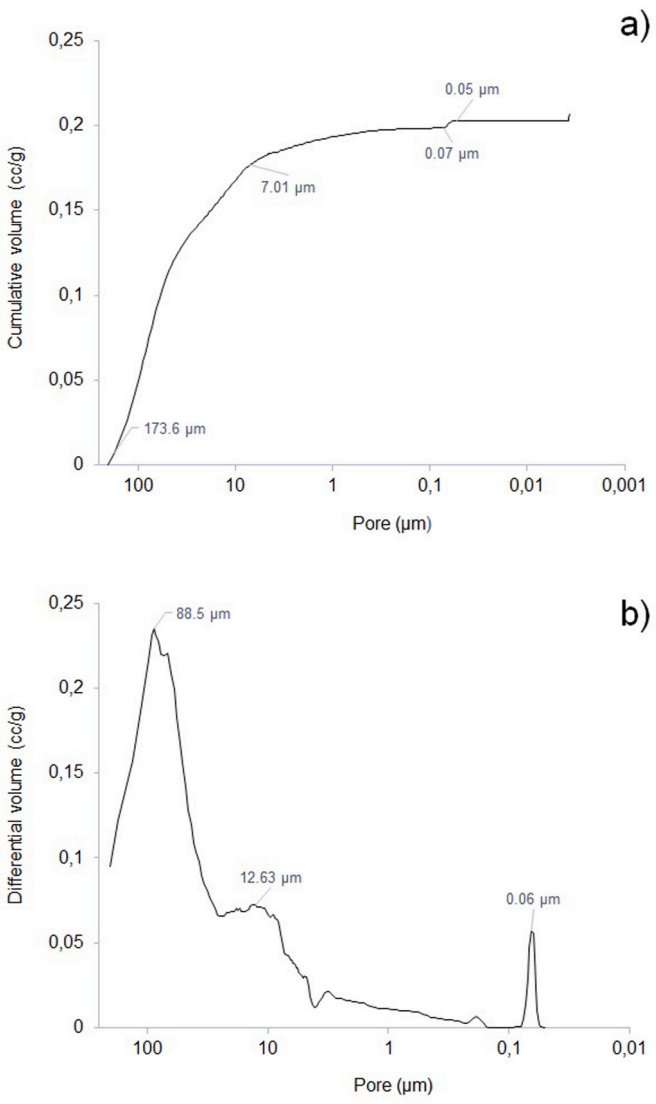

Fig. 3. Mercury porosimetry curves: (a) cumulative and (b) differential intruded volume vs. pore diameter.

was around 0.56–0.67 MPa after treatment. The etching process did not alter the scaffolds' mechanical properties.

3.3. Scaffolds' in vitro bioactivity

The acid-etched scaffolds' *in vitro* bioactivity was tested by soaking them in SBF solution for 12 h, and 1, 7 and 14 days. After 12 h (Fig. 7A), many precipitates were distributed on scaffolds' surface, especially in the grooved areas. The EDX analysis of precipitates revealed that they were composed of Ca, P, and chlorine (Cl), and their Ca/P ratio was of about 1.5, which indicates the presence of chlorapatite precipitates. After 1 day (Fig. 7B), apatite precipitates started to form a layer on top of the grooved areas, with a Ca/P ratio of 1.5–1.6 depending on the area. After 7 days (Fig. 7C) and 14 days (Fig. 7D), no bioactivity was observed on scaffolds, probably due to the dissolution of the external layer along with the newly formed apatite precipitates and, consequently, hexagonal grains of pyrophosphate from the core, with a Ca/P ratio of 1.0, were then visible.

To enhance the bioactivity of the etched scaffolds, they were coated again with a new composition doped with strontium (Sr^{2+}) ions to improve their bioactive capacity. Fig. 8 (A – C) shows the SEM images of the scaffolds obtained after immersion in SBF for 7, 14 and 21 days. After 7 days, no bioactivity was observed on scaffolds, but after 14, and especially after 21 days (Fig. 8C), spherical precipitates were deposited on the scaffolds' surface. The EDX analysis revealed that precipitates were composed of Ca and P and their Ca/P ratio was of 1.69, which corresponds to the stoichiometric value of hydroxyapatite (HA) ($Ca_{10}(PO_4)_6(OH)_2$), modified by the presence of Sr, confirming that the scaffolds' bioactive capacity was enhanced after 7 days thanks to the incorporation of strontium.

The changes in the Ca, Si and P ion concentrations in SBF after the different immersion times were measured by ICP-OES (Fig. 9). In scaffolds doped with Sr, for the first 7 days, the calcium concentration in SBF slightly lowered. After this time, however, its concentration in the medium started increasing because Ca ions were released from the scaffolds and went from a concentration of 45.08 mg/L on day 7, to a maximum concentration of 87.13 mg/L on the last assay day. The Si and P ions displayed the exact opposite behaviour, while the silicon concentration in SBF continuously rose throughout the experiment and went from an initial concentration of only 0.09 mg/L to one of 36.31 mg/L as Si ions were released to the medium, the phosphorus concentration went from 22.89 mg/L to 1.02 mg/L as it was adsorbed in the scaffolds. These changes are related to the formation of apatite precipitates on scaffolds' surface, especially after 14 and 21 days.

4. Discussion

In the present study, 3D porous ceramic scaffolds were fabricated by the sol-gel method in combination with the polymeric sponge replication method following the procedure previously described in the literature [24]. This methodology allows us to obtain ceramic scaffolds with interconnected porosity by a simple low-cost fabrication process. Striking a balance between the material's mechanical resistance and its bioactive capacity is very important, which is why we developed multilayer scaffolds, as it is well-known that CaP materials with high mechanical properties like calcium pyrophosphate are barely bioactive, whereas bioactive materials like tricalcium phosphate (TCP) are very soluble and offer poor mechanical resistance [26,27].

Firstly, the inner layers of the scaffolds, known as "core", were fabricated and characterised. The multilayer scaffolds' core had interconnected porosity and, according to the XRD pattern, it was mainly composed of calcium pyrophosphate. Having obtained the core, it was coated with a new composition in which sol-gel reactants were mixed at a Ca/P atomic ratio of 1.3 to obtain a mixture of the calcium pyrophosphate and TCP phases and, therefore, greater bioactive capacity. Fig. 1B shows the final multilayer scaffolds' microstructure. Compared to the core alone, the final multilayer scaffolds had a smoother surface with some hexagonal pyrophosphate grains, probably due to a higher presence of TCP on the external layers.

The scaffolds' chemical and mineralogical composition analysed by SEM-EDX and XRD showed that, as expected, scaffolds were composed mainly of two phases: a larger calcium pyrophosphate ($Ca_2O_7P_2$) phase and a smaller β-tricalcium phosphate ($Ca_3(PO_4)_2$) one (Fig. 2A). The EDX results revealed a Ca/P ratio of about 1.24, which comes close to 1.3, the intermediate Ca/P ratio between TCP and pyrophosphate, further confirming that the scaffolds' surface presented a mixture of both phases.

The final multilayer scaffolds presented interconnected porosity with a total porosity value of 36.95% as determined by the Mercury Porosimetry Technique (Fig. 3). A high volume of mercury intrusion was observed in pores whose size was between 173.6 µm and 7.01 µm, followed by minor mercury intrusion, which corresponded to a pore size between 0.07 µm and 0.05 µm (Fig. 3A). More specifically, the largest intrusion volume corresponded to interparticle spaces (32.34%), with a pore size of about 88.5 µm and a few pores of around 12.63 µm. The small mercury intrusion volume corresponded to intraparticle spaces (4.60%), with a pore size of 0.06 µm (Fig. 3B). The importance of porosity in bone scaffolds has been widely studied, with authors reporting that 90% porosity and a pore size from 50 to 100 µm are

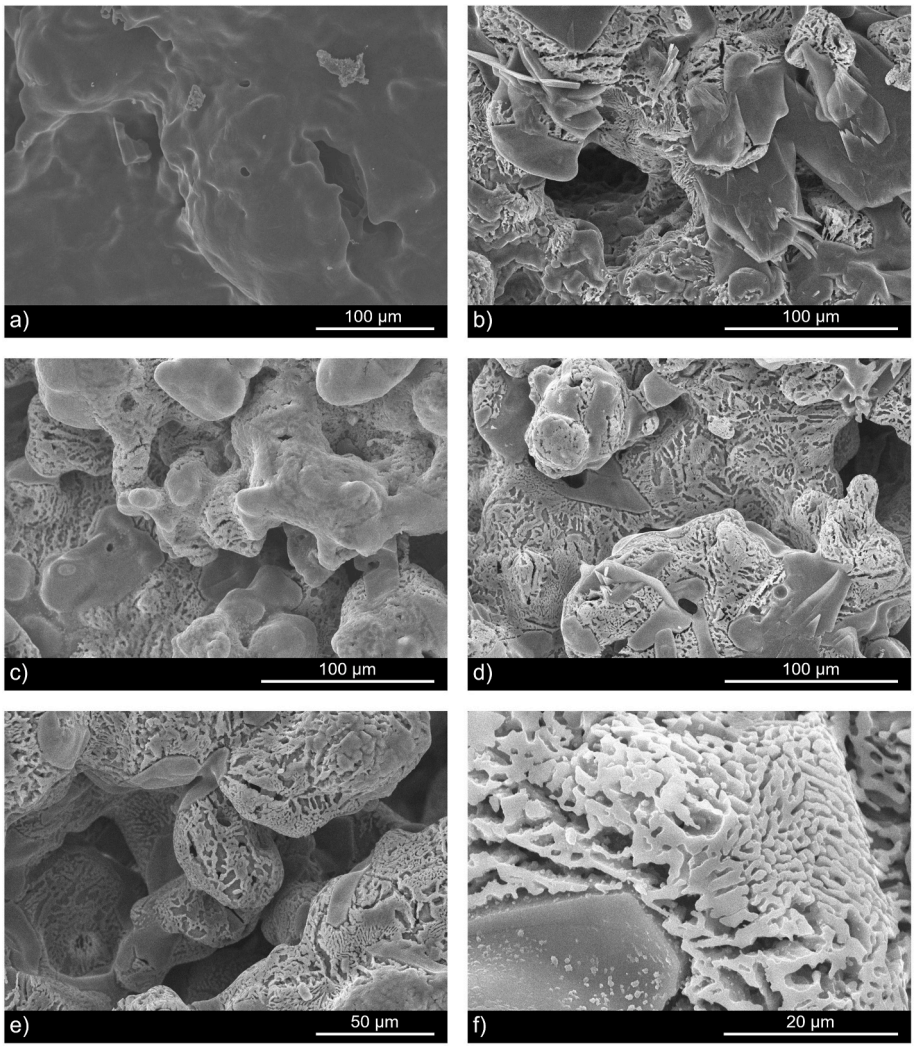

Fig. 4. SEM micrographs of the scaffolds' surface after different etching times and concentrations: (a) Control; (b) 10% for 90 s; (c) 5% for 90 s; (d, e) 3% for 90 s and 120 s respectively and (f) detail of the ridges and grooves at high magnification.

necessary to ensure a proper bone tissue ingrowth in porous scaffolds [5,6]. Microporosity (<10 µm) is also essential to ensure a good ionic exchange and protein adsorption [3]. Our scaffolds presented an adequate pore size between 88.5 µm and 0.06 µm, although their total porosity of 36.95% was lower than the optimal value of 80–90% stated in the literature.

The multilayer CaP scaffolds were chemically etched to modify their surface topography in order to introduce a topographical pattern in the form of ridges and grooves. Traditionally, ceramic materials like, HA and TCP, have been used as coatings on materials with greater mechanical strength, such as titanium and its alloys, or synthetic polymers like poly lactic-*co*-glycolic acid (PLGA), on which the modification of their surface morphology has been previously exerted to increase their bioactivity, while maintaining these material's desired mechanical properties. For instance, Akasaka et al. [28] produced grooves on a polydimethylsiloxane (PDMS) mold and coated them with α-TCP to study the effect of different patterns on the adhesion of SaOS-2 cells. Similarly, Lu et al. [29] fabricated microgrooved surfaces by photolithography and coated them with HA to study their effect on osteoblast behaviour. There have been a few studies reporting the modification of the surface topography of ceramic materials [7,8], but in general, currently available nano-/microfabrication techniques can only introduce topographic patterns into planar surfaces, which makes it extremely difficult to modify the surface of three-dimensional porous materials, and especially, to create well-defined topographic patterns directly on the surface of ceramics.

Chemical etching has already been used to increase ceramic scaffolds' surface roughness, porosity, and interconnectivity [27,30,31]. However, as ceramic materials are more fragile than polymers or metals given their brittleness, it is more challenging to produce patterned surfaces on CaP scaffolds. Doi et al. [27] employed chemical etching to increase the surface roughness of porous HA, observing higher bone formation after *in vivo* implantation in a rabbit femur. The topographical modification is made as a result of the difference in susceptibility of the crystallographic phases composing the scaffolds and is directly related to the etchant concentration and etching time. The advantage of chemical etching over other nano-/microfabrication techniques is that it can be used in ceramic materials and is a simple cost-effective method with good scalability. To the best of our knowledge, chemical etching has not been previously used to introduce a grooved pattern into 3D porous CaP scaffolds.

This technique needs to be carefully standardised to etch multiphase ceramic materials as their individual phases have different chemical susceptibilities, which is why different acetic acid (CH_3COOH) concentrations were tested before finding the optimal conditions to introduce ridges and grooves that were uniformly distributed on scaffolds' surface, avoiding the over-etching of the material at the same time. Initially a 10% acetic acid concentration was used for 90 s (Fig. 4B), but only a

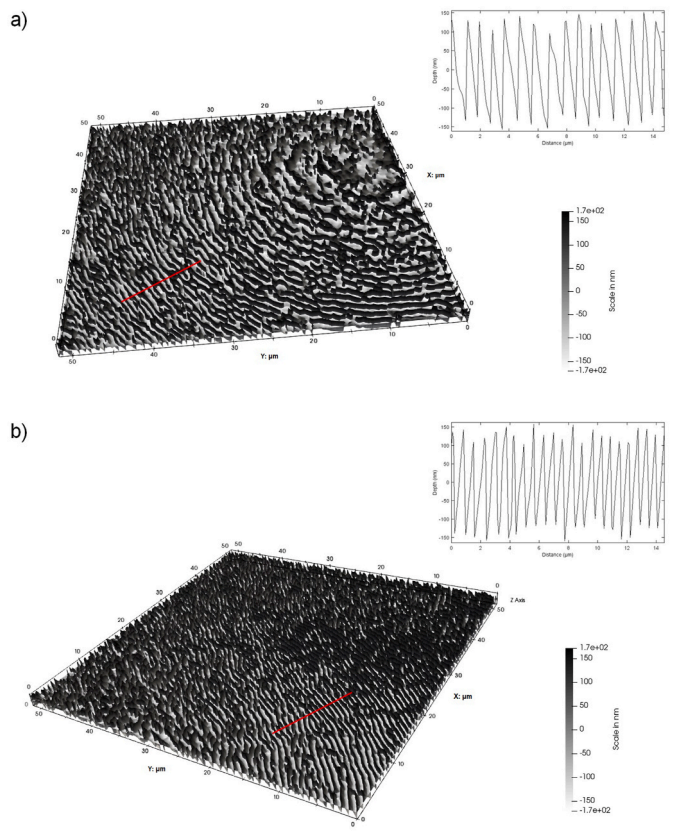

Fig. 5. Three-dimensional surface profiles and height profiles of the chemically etched scaffolds by DHM at different times: (a) 60s and (b) 120s.

small amount of not very well-defined ridges and grooves was observed on the surface. A concentration of 5% acetic acid was also tested, but after 90 s (Fig. 4C) only a few ridges and grooves were visible on the scaffolds' surface. We prolonged the etching time to 120 s at the same concentration, but no ridges and grooves were observed. Finally, when scaffolds were etched with 3% acetic acid for 90 s (Fig. 4D), and especially 120 s (Fig. 4E), a large number of well-defined ridges and grooves were uniformly distributed along scaffolds' surface. Other etching times, 30 and 60 s, were also tested for the 3% acetic acid concentration, but the ridges and grooves obtained were not distributed as uniformly as those obtained after 90 and 120 s.

When comparing the scaffolds' mineralogical composition before and after chemical etching (Fig. 2), the diffractograms slightly differed. The peaks corresponding to the calcium pyrophosphate phase were smaller after etching, especially the main peak at 30 2theta, while the peaks for the β-TCP phase were more prominent. The Ca/P ratio was altered as well and went from 1.24 on the untreated scaffolds to a slightly higher value of 1.31 on the etched scaffolds. The Ca/P ratio in the grooved areas came close to 1.5; that is, the stoichiometric value for β-tricalcium phosphate. Taking this together, we hypothesised that the calcium pyrophosphate phase (Ca/P ratio of 1.0) located on the external layer was selectively etched off the scaffolds' surface by the etching process, which resulted in grooves forming on the surface where it was originally present. We believe that both calcium pyrophosphate and β-tricalcium phosphate are distributed on the surface as alternating lamellae, forming a lamellar structure which, together with their different susceptibility to chemical etching, are responsible for the formation of ridges and grooves on the scaffolds' surface.

The ridges and grooves produced by the chemical etching treatment were characterised by Digital Holographic Microscopy (Fig. 5) and SEM (Fig. 6) to determine their main dimensions, width and depth. Fig. 5 depicts the 3D surface profiles of the etched scaffolds after 60 s (Fig. 5A) and 120 s (Fig. 5B). The produced ridges and grooves were on the nano-/micrometric scale and had slightly different dimensions between etching times. When comparing the height profiles for each time, we found how ridges and grooves became narrower and deeper with longer etching times. Altogether, the width of ridges and grooves was between 900 nm–1.5 μm, and the depth of grooves was around 200 nm–300 nm. The width of our ridges and grooves was very similar to those obtained by Akasaka et al. [28], who reported that more human osteoblast-like cells SaOS-2 were attached to 2 μm wide ridges and grooves compared to planar surfaces. Moreover, SaOs-2 cells exhibited an elongated morphology on the grooved surfaces. The depth of our grooves was also similar to that reported by Azeem et al. [32]. In their work, a groove depth of 306 nm was shown to influence the morphology and alignment of osteoblasts better than the 35 nm deep grooves, and also on the planar surfaces. These studies support the notion that the dimensions of the ridges and grooves herein obtained could positively promote osteoblast adhesion, alignment, and elongation.

Scaffolds' compressive strength before chemical etching was about 0.46–0.67 MPa, while their resistance was 0.56–0.67 MPa after treatment. Even if the calcium pyrophosphate from the external layer was dissolved, the etching process did not compromise the scaffolds' mechanical properties. These results are similar to other studies performed with ceramic scaffolds with similar compressive strength values of 0.18–0.40 MPa [24] and 0.3–0.4 MPa [33]. The mechanical strength of human sponge bone ranges from 0.2 to 4 MPa and even after chemical etching our scaffolds' compressive strength fell within these values. Furthermore, this mechanical resistance is expected to increase over time as new bone grows into scaffolds [27,33].

The *in vitro* bioactivity of the etched scaffolds was tested by soaking them in SBF as established by Kokubo et al. [25] for 12 h, and 1, 7 and 14 days (Fig. 7) to determine if the etching process affected their bioactive capacity. This *in vitro* bioactivity is determined by an apatite layer forming on the material's surface when it comes into contact with SBF [34]. After 1 day, ridges and grooves were still observed on scaffolds' surface and in some areas, were covered by a layer of apatite precipitates

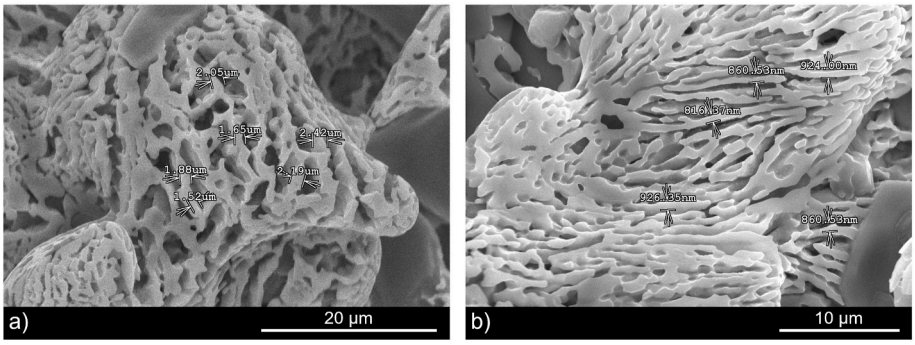

Fig. 6. SEM micrograph of the ridges width at different times: (a) 60s and (b) 120s.

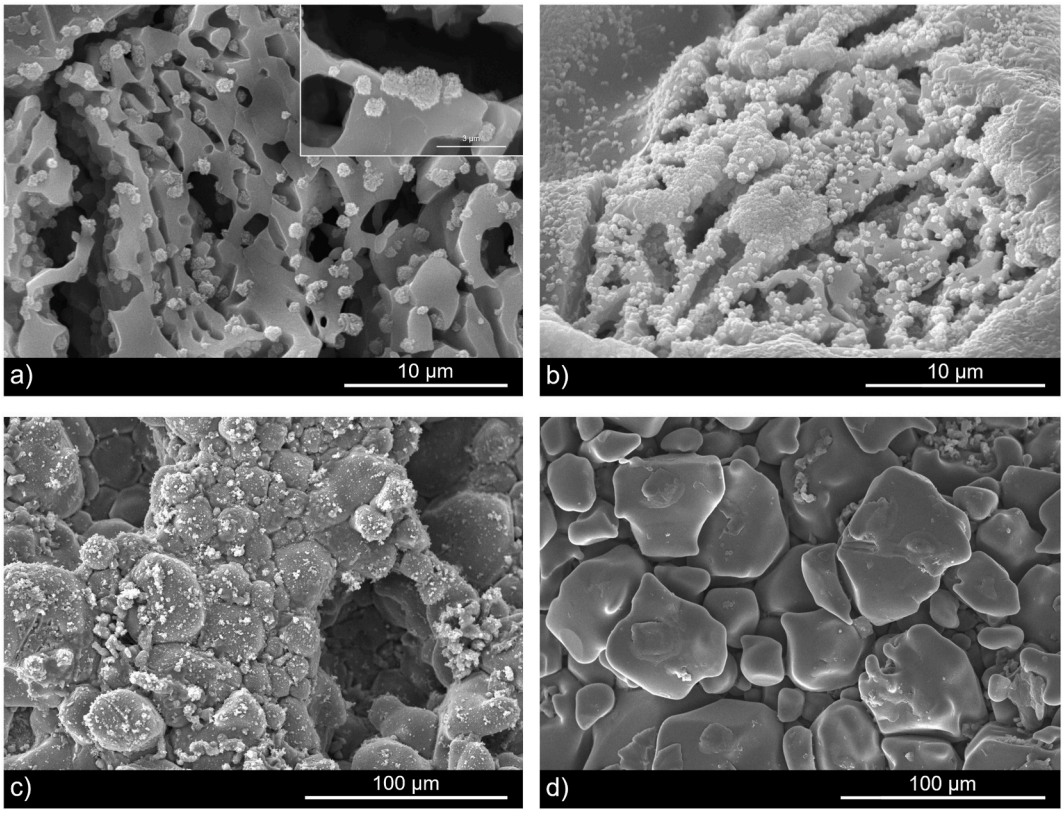

Fig. 7. SEM micrographs of chemically etched scaffolds soaked in SBF for: (a) 12 h; (b) 1 day; (c) 7 days and (d) 14 days.

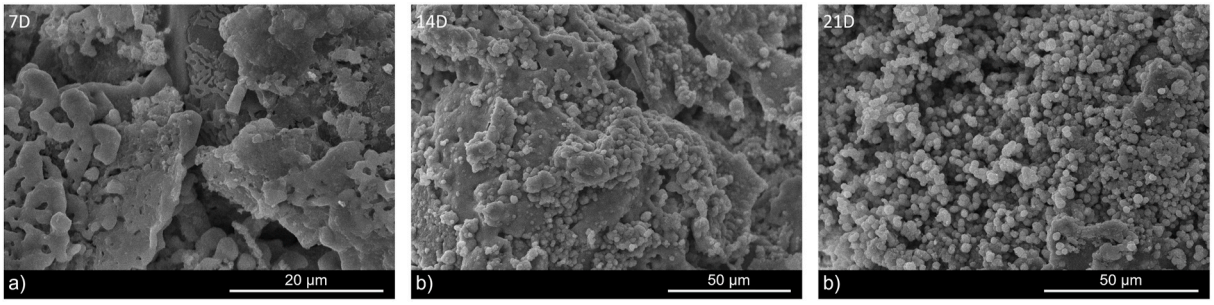

Fig. 8. SEM micrographs of strontium-doped scaffolds soaked in SBF for: (a) 7 days; (b) 14 days and (c) 21 days.

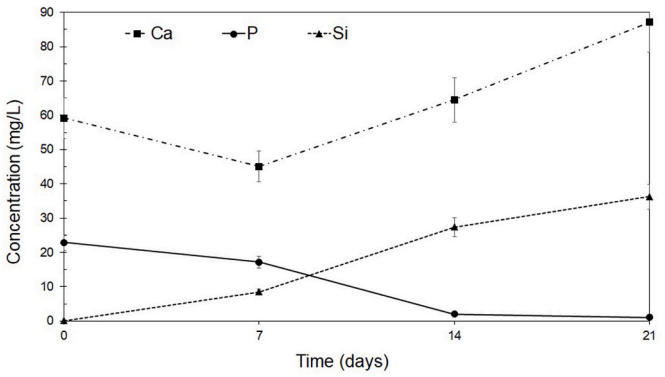

Fig. 9. Changes in calcium (Ca), silicon (Si) and phosphorus (P) ion concentration after immersion in SBF for 7, 14 and 21 days.

(Fig. 7B). The EDX analysis of precipitates showed that they were composed of Ca, P and Cl with a Ca/P ratio of 1.5–1.6 depending on the area. These precipitates could be chlorapatite ($Ca_5(PO_4)_3Cl$; Ca/P ratio of 1.67), which is a type of apatite with chloride as the dominant anion. Their Ca/P ratio was lower than that of stoichiometric chlorapatite, probably modified by the presence of β-TCP in the grooved areas. After 7 days in SBF (Fig. 7C), only a few ridges and grooves were still observed on scaffolds' surface, likely due to the dissolution of the remaining β-TCP on the external layer. Only the calcium pyrophosphate from the core, in the form of hexagonal grains, remained. Therefore, no bioactivity was observed due to the inhibitory effect of pyrophosphate in the apatite precipitation process [35]. Some precipitates were present on the surface and, according to the EDX analysis, they were composed of magnesium (Mg), sodium (Na) and chlorine, and were probably salt deposits that originated from the SBF solution. Similarly, after 14 days (Fig. 7D), no bioactivity was observed as the external layer had been completely dissolved and the surface was entirely covered by hexagonal grains of calcium pyrophosphate, with a Ca/P ratio of 1.0.

We believe that after 1 day, the remaining β-TCP on the external

layer of etched scaffolds, which formed the ridges, started to dissolve along with the chlorapatite precipitates. For this reason, after 7 days only a few ridges and grooves were still present on scaffolds' surface, and none were found after 14 days. Due to the dissolution of calcium pyrophosphate after etching, β-TCP could have been more exposed to SBF and dissolved more rapidly than on the non-etched scaffolds. We tested scaffolds' bioactivity for only 12 h, as it could be possible that apatite precipitation occurred mainly during these first few hours before β-TCP started to dissolve. After 12 h (Fig. 7A), many chlorapatite precipitates, with a Ca/P ratio of about 1.5, were visible mainly on top of the grooved areas. It would seem that at some point between 12 and 24 h, the dissolution of the external layer started, especially in the grooved areas, as they were mostly composed of β-TCP, having as a consequence the dissolution of the newly formed apatite precipitates. Therefore, no bioactivity was observed after 7 and 14 days as only the calcium pyrophosphate from the core remained, which inhibited new apatite precipitation.

For this reason, scaffolds were coated again with the same composition used for the external layers but dope with Sr ions, as it has been previously described that its incorporation into ceramic scaffolds can increase their osteogenic and bioactive capacity [3,36]. Strontium-doped scaffolds were then soaked in SBF for 7, 14 and 21 days (Fig. 8). After 7 days (Fig. 8A), no bioactivity was observed on scaffolds' surface, and some ridges and grooves were still observed on the surface below the new layer doped with Sr. At 14 days (Fig. 8B), many spherical precipitates were noted on scaffolds' surface, as was the case especially at 21 days (Fig. 8C), when the number of spherical particles significantly rose and covered the whole surface. The SEM-EDX analysis of scaffolds showed that precipitates were composed of Ca and P and their Ca/P ratio was 1.69, which was slightly higher than the stoichiometric value of hydroxyapatite, with a Ca/P ratio of 1.67, probably due to the presence of Sr ions [36]. In any case, the strontium-doped scaffolds displayed better bioactive capacity and their bioactivity increased with immersion time.

Hydroxyapatite precipitation is directly related to the ionic exchange between scaffolds and SBF and, for this reason, changes in the Ca, Si and P ion concentrations after the different immersion times in SBF were determined by Inductively Coupled Plasma Optical Emission Spectrometry (ICP-OES) (Fig. 9). For scaffolds doped with Sr, at the beginning of the assay, the concentration of the Ca ions slightly lowered for the first 7 days. After this time, it continuously increased until the end of the experiment, and went from a minimum of 45.08 mg/L to a maximum of 87.13 mg/L. This was probably due to Ca ions from the scaffold being released, and also to the dissolution of the new unstable apatite layer, which precipitated after 7 days in SBF, especially between 14 and 21 days and, therefore, increased the Ca concentration. This increased HA precipitation after 7 days also correlated with a lower P ion concentration in the medium. Phosphorous in SBF constantly lowered throughout the experiment from 22.89 mg/L to a minimum value of 1.02 mg/L as it was adsorbed in scaffolds and the new apatite layer formed. As the assay progressed, Si ions were constantly released from the scaffolds, from an initial concentration of 0.09 mg/L to a maximum one of 36.31 mg/L in SBF, which likely indicates the scaffolds' dissolution. The dissolution of the calcium pyrophosphate from the external layer could greatly improve our scaffolds' bioactivity, not only by the formation of ridges and grooves that positively promote cell behaviour, but also by the dissolution of pyrophosphate itself as its inhibitory role in the apatite precipitation process has been well established [35]. In future works, it would be of interest to obtain more stable ridges and grooves that could last longer before starting to dissolve after immersion in SBF.

The effect of surface topographies like ridges and grooves on the cellular behaviour of osteoblasts and hMSCs has been extensively studied in the last few decades [29,37]. Topographic patterns in the form of ridges and grooves have attracted considerable attention owing to their similarity to the collagen fibres composing the bone ECM. According to the literature, the dimensions (width and depth) of ridges and grooves are a critical factor for inducing contact guidance; that is, to promote adhesion, alignment, elongation, and migration along the pattern [38,39]. It is known that cells in an ordered alignment are more likely to differentiate into an osteogenic phenotype [5,6] and, therefore, an optimal ridge/groove dimension that promotes this alignment as well as a good cellular response, both *in vitro* and *in vivo*, needs to be determined.

According to other authors, the pattern needs to have similar dimensions to that of the cell to effectively guide their alignment [39–41]. Furthermore, this contact guidance effect is not only size-dependent, but also cell-type dependent as different cellular types are known to have varying sensitivities [29,38], which must be considered when designing patterned surfaces.

Regarding the effect of topography on osteoblast behaviour, many studies have been conducted using different pattern sizes within the micrometric range. Kirmizidis et al. [14] studied the effect of micrometric grooved patterns (10–30 μm in width; 7 μm in depth) on osteoblast behaviour. They found that osteoblasts not only adhere and align according to grooves, but also a marker of osteoblasts differentiation, alkaline phosphatase activity (ALP), was observed. Lu et al. [40] also investigated the groove guidance effect on SaOS-2 cells using micrometric dimensions (4–38 μm in width; 2–10 μm in depth). They found that the guidance effect gradually weakened as groove width increased. It would appear that narrow grooves are better at controlling cellular behaviour than wide ones [28,29].

Although no consensus has been reached between different studies about the optimal dimensions needed to induce a proper osteoblasts response, some authors believe that cells may respond better to topographies within the nanometric range, probably because the ECM is comprised of nanosized collagen fibrils of 50–30 nm [42], and also because cell filopodia (250–400 nm), which are responsible for the initial cell attachment to the surface, better perceives smaller dimensions [38]. Nanometric ridges and grooves could, therefore, better resemble the "*in vivo*" interaction of cells with the ECM. For instance, Lamers et al. [37] observed that nanometric ridges/grooves within the natural bone ECM range were able to induce osteoblast alignment down to a width of 75 nm and a depth of 33 nm. These authors also found that osteogenic markers like ALP and osteocalcin (OCN) were up-regulated on nanometric grooved surfaces. Watari et al. [20] also observed the enhanced osteogenic differentiation of hMSCs when cultured on nanoscale (100–400 nm) ridges and grooves. Nanoscale features appear to produce more efficient adhesion, alignment and elongation than microscale patterns [13,43]. Although many studies have focused on the effect of pattern width on cellular behaviour, groove depth has also been found to influence cell alignment, with 150 nm grooves inducing a statistically higher degree of alignment than 50 nm grooves [44].

Several studies have been conducted to elucidate how cells respond to topography but, the mechanism by which topographical cues modulate cell behaviour is still not fully understood. Grooved patterns can promote the adsorption of adhesion proteins like fibronectin and vitronectin and enhance integrin activation, which are transmembrane receptors that together with these proteins mediate the cell-ECM adhesion process through the formation of focal adhesions (FAs) [42,45]. This enhancement of the adhesion process can, in turn, influence other cellular functions like cell proliferation and differentiation, which can lead to increased osteogenesis [46]. Moreover, it has also been reported that changes in cell morphology can regulate the cellular differentiation process [39]. Grooved topography can induce cell elongation, which can subsequently induce changes in the cytoskeleton and nucleus through cytoskeletal tensions. These alterations in the nucleus can lead to changes in gene expression and might, therefore, influence cell osteogenic differentiation [20,32].

When designing biomaterials to be used in bone tissue engineering, it is desirable to make attempts to mimic the original bone tissue conditions. Most tissues possess features ranging from the macro-to the nanoscale which, in turn, affect cell-tissue interactions. The

incorporation of surface topographical patterns into ceramic materials is a topic of interest because, as we have previously discussed, it is known that they can positively promote cellular behaviour, further increasing the porous CaP scaffolds' osteoinductive capacity. To date, researchers have fabricated patterned surface mainly on polymers and metals, thanks to technologies like photolithography, electrospinning, electron beam lithography and colloidal lithography [38]. Better fabrication techniques are still required to produce complex surface patterns, especially on other materials like ceramics. Chemical etching is a low-cost process that has allowed us to obtain highly reproducible topographic surface patterns in the form of ridges and grooves and, more importantly, it can be used in three-dimensional porous ceramic scaffolds.

The ridges and grooves herein fabricated were nano-/micrometric-sized (900–1.5 μm in width; 200–300 nm in depth) and, according to the previous literature, we believe that our patterned scaffolds could better resemble the ECM *in vivo* architecture, improving cell-material interactions [47] and promoting osteoblasts and hMSC adhesion, alignment, elongation, and differentiation [20,28,39], better enhancing their osteogenic capacity than conventional scaffolds.

5. Conclusion

Considering the surface topography effect on cell behaviour, this study focused on manufacturing a grooved structure on 3D ceramic porous scaffolds' surface. By means of a simple low-cost chemical etching treatment, a topographical pattern in the form of ridges and grooves was introduced in scaffolds' surface without affecting their structural integrity.

Our patterned scaffolds were composed mainly of a mixture of two different phases: a calcium pyrophosphate one and a β-tricalcium phosphate phase. Both the difference in the constituent crystallographic phases' susceptibility to etching, together with their lamellar structure, were responsible for the formation of the grooved pattern as the calcium pyrophosphate on the external layer was etched off the surface.

The dimensions of ridges and grooves were around 900 nm–1.5 μm in width and 200–300 nm in depth, and they slightly varied with the concentration and etching time. The best results were obtained with 3% acetic acid for 120 s. Furthermore, scaffolds doped with Sr were highly bioactive after 14 and 21 days in SBF and the etching process did not affect their mechanical resistance.

Ceramic scaffolds' surface topography modification represents a promising strategy to improve their *in vivo* osteogenic capacity compared to conventional scaffolds used in bone tissue engineering.

Funding source

This research did not receive any specific grant from funding agencies in the public, commercial, or not-for-profit sectors.

Declaration of competing interest

The authors declare that they have no known competing financial interests or personal relationships that could have appeared to influence the work reported in this paper.

References

[1] I. Denry, L.T. Kuhn, Design and characterization of calcium phosphate ceramic scaffolds for bone tissue engineering, Dent. Mater. 32 (2016) 43–53, https://doi.org/10.1016/j.dental.2015.09.008.
[2] S.I. Roohani-Esfahani, S. Nouri-Khorasani, Z. Lu, R. Appleyard, H. Zreiqat, The influence hydroxyapatite nanoparticle shape and size on the properties of biphasic calcium phosphate scaffolds coated with hydroxyapatite-PCL composites, Biomaterials 31 (2010) 5498–5509, https://doi.org/10.1016/j.biomaterials.2010.03.058.
[3] D. Xiao, J. Zhang, C. Zhang, D. Barbieri, H. Yuan, L. Moroni, G. Feng, The role of calcium phosphate surface structure in osteogenesis and the mechanisms involved, Acta Biomater. 106 (2020) 22–33, https://doi.org/10.1016/j.actbio.2019.12.034.
[4] N. Robin, R. Zang, K.K. Yang, N. Liu, S.T. Yang, Three-dimensional fibrous scaffolds with microstructures and nanotextures for tissue engineering, RSC Adv. 2 (2012) 10110–10124, https://doi.org/10.1039/c2ra21085a.
[5] L. Zhu, D. Luo, Y. Liu, Effect of the nano/microscale structure of biomaterial scaffolds on bone regeneration, Int. J. Oral Sci. 12 (2020), https://doi.org/10.1038/s41368-020-0073-y.
[6] Y. Du, J.L. Guo, J. Wang, A.G. Mikos, S. Zhang, Hierarchically designed bone scaffolds: from internal cues to external stimuli, Biomaterials 218 (2019), https://doi.org/10.1016/j.biomaterials.2019.119334.
[7] D.D. Deligianni, N.D. Katsala, P.G. Koutsoukos, Y.F. Missirlis, Effect of surface roughness of hydroxyapatite on human bone marrow cell adhesion, proliferation, differentiation and detachment strength, Biomaterials 22 (2000) 87–96, https://doi.org/10.1016/S0142-9612(00)00174-5.
[8] E.A. dos Santos, M. Farina, G.A. Soares, K. Anselme, Chemical and topographical influence of hydroxyapatite and β-tricalcium phosphate surfaces on human osteoblastic cell behavior, J. Biomed. Mater. Res. 89 (2009) 510–520, https://doi.org/10.1002/jbm.a.31991.
[9] M.J. Dalby, M.O. Riehle, S.J. Yarwood, C.D.W. Wilkinson, A.S.G. Curtis, Nucleus alignment and cell signaling in fibroblasts: response to a micro-grooved topography, Exp. Cell Res. 284 (2003) 272–280, https://doi.org/10.1016/S0014-4827(02)00053-8.
[10] S. Lenhert, M.B. Meier, U. Meyer, L. Chi, H.P. Wiesmann, Osteoblast alignment, elongation and migration on grooved polystyrene surfaces patterned by Langmuir-Blodgett lithography, Biomaterials 26 (2005) 563–570, https://doi.org/10.1016/j.biomaterials.2004.02.068.
[11] A.I. Teixeira, G.A. Abrams, P.J. Bertics, C.J. Murphy, P.F. Nealey, Epithelial contact guidance on well-defined micro- and nanostructured substrates, J. Cell Sci. 116 (2003) 1881–1892, https://doi.org/10.1242/jcs.00383.
[12] S. Koo, R. Muhammad, G.S.L. Peh, J.S. Mehta, E.K.F. Yim, Micro- and nanotopography with extracellular matrix coating modulate human corneal endothelial cell behavior, Acta Biomater. 10 (2014) 1975–1984, https://doi.org/10.1016/j.actbio.2014.01.015.
[13] M.J.P. Biggs, R.G. Richards, S. McFarlane, C.D.W. Wilkinson, R.O.C. Oreffo, M. J. Dalby, Adhesion formation of primary human osteoblasts and the functional response of mesenchymal stem cells to 330 nm deep microgrooves, J. R. Soc. Interface 5 (2008) 1231–1242, https://doi.org/10.1098/rsif.2008.0035.
[14] G. Kirmizidis, M.A. Birch, Microfabricated grooved substrates influence cell–cell communication and osteoblast differentiation *in vitro*, Tissue Eng. 15 (2009) 1427–1436, https://doi.org/10.1089/ten.tea.2008.0137.
[15] D. Khang, J. Choi, Y.M. Im, Y.J. Kim, J.H. Jang, S.S. Kang, T.H. Nam, J. Song, J. W. Park, Role of subnano-, nano- and submicron-surface features on osteoblast differentiation of bone marrow mesenchymal stem cells, Biomaterials 33 (2012) 5997–6007, https://doi.org/10.1016/j.biomaterials.2012.05.005.
[16] A.E. Loiselle, L. Wei, M. Faryad, E.M. Paul, G.S. Lewis, J. Gao, A. Lakhtakia, H. J. Donahue, Specific biomimetic hydroxyapatite nanotopographies enhance osteoblastic differentiation and bone graft osteointegration, Tissue Eng. 19 (2013) 1704–1712, https://doi.org/10.1089/ten.tea.2012.0560.
[17] P. Wang, L. Zhao, J. Liu, M.D. Weir, X. Zhou, H.H.K. Xu, Bone tissue engineering via nanostructured calcium phosphate biomaterials and stem cells, Bone Res. 2 (2014), https://doi.org/10.1038/boneres.2014.17.
[18] M. Irving, M.F. Murphy, F. Lilley, P.W. French, D.R. Burton, S. Dixon, M.C. Sharp, The use of abrasive polishing and laser processing for developing polyurethane surfaces for controlling fibroblast cell behaviour, Mater. Sci. Eng. C 71 (2017) 690–697, https://doi.org/10.1016/j.msec.2016.10.067.
[19] Y.L. Jung, H.J. Donahue, Cell sensing and response to micro- and nanostructured surfaces produced by chemical and topographic patterning, Tissue Eng. 13 (2007) 1879–1891, https://doi.org/10.1089/ten.2006.0154.
[20] S. Watari, K. Hayashi, J.A. Wood, P. Russell, P.F. Nealey, C.J. Murphy, D. C. Genetos, Modulation of osteogenic differentiation in hMSCs cells by submicron topographically-patterned ridges and grooves, Biomaterials 33 (2012) 128–136, https://doi.org/10.1016/j.biomaterials.2011.09.058.
[21] M.M. McCafferty, G.A. Burke, B.J. Meenan, Calcium phosphate thin films enhance the response of human mesenchymal stem cells to nanostructured titanium surfaces, J. Tissue Eng. (2014) 5, https://doi.org/10.1177/2041731414537513.
[22] B. Zhu, Q. Lu, J. Yin, J. Hu, Z. Wang, Alignment of osteoblast-like cells and cell-produced collagen matrix induced by nanogrooves, Tissue Eng. 11 (2005) 825–834, https://doi.org/10.1089/ten.2005.11.825.
[23] D. Nadeem, C.A. Smith, M.J. Dalby, R.M. Dominic Meek, S. Lin, G. Li, B. Su, Three-dimensional CaP/gelatin lattice scaffolds with integrated osteoinductive surface topographies for bone tissue engineering, Biofabrication 7 (2015), https://doi.org/10.1088/1758-5090/7/1/015005.
[24] P. Ros-Tárraga, A. Murciano, P. Mazón, S.A. Gehrke, P.N. de Aza, New 3D stratified Si-Ca-P porous scaffolds obtained by sol-gel and polymer replica method: microstructural, mineralogical and chemical characterization, Ceram. Int. 43 (2017) 6548–6553, https://doi.org/10.1016/j.ceramint.2017.02.081.
[25] T. Kokubo, H. Takadama, How useful is SBF in predicting in vivo bone bioactivity? Biomaterials 27 (2006) 2907–2915, https://doi.org/10.1016/j.biomaterials.2006.01.017.
[26] S. Samavedi, A.R. Whittington, A.S. Goldstein, Calcium phosphate ceramics in bone tissue engineering: a review of properties and their influence on cell behavior, Acta Biomater. 9 (2013) 8037–8045, https://doi.org/10.1016/j.actbio.2013.06.014.

[27] K. Doi, Y. Abe, R. Kobatake, Y. Okazaki, Y. Oki, Y. Naito, W. Prananingrum, K. Tsuga, Novel development of phosphate treated porous hydroxyapatite, Materials 10 (2017), https://doi.org/10.3390/ma10121405.
[28] T. Akasaka, H. Miyaji, K. Naoyuki, A. Yokoyama, Y. Yoshida, Adhesion of osteoblast-like cells (Saos-2) on micro-/submicro-patterned apatite scaffolds fabricated with apatite cement paste by micro-molding, Nano Biomed. 8 (2016) 112–122, https://doi.org/10.11344/nano.8.112.
[29] X. Lu, Y. Leng, Comparison of the osteoblast and myoblast behavior on hydroxyapatite microgrooves, J. Biomed. Mater. Res. B Appl. Biomater. 90 B (2009) 438–445, https://doi.org/10.1002/jbm.b.31304.
[30] S. Lee, S. Yang, I. Bajpai, I.K. Kang, S. Kim, Enhancement of the pore interconnectivity and porosity of calcium phosphate scaffolds by acid-etching method, Acta Metall. Sin. (English Lett.) 28 (2015) 1109–1116, https://doi.org/10.1007/s40195-015-0301-1.
[31] C. Gao, J. Zhuang, P. Li, C. Shuai, S. Peng, Preparation of micro/nanometer-sized porous surface structure of calcium phosphate scaffolds and the influence on biocompatibility, J. Mater. Res. 29 (2014) 1144–1152, https://doi.org/10.1557/jmr.2014.100.
[32] A. Azeem, A. English, P. Kumar, A. Satyam, M. Biggs, E. Jones, B. Tripathi, N. Basu, J. Henkel, C. Vaquette, N. Rooney, G. Riley, A. O'Riordan, G. Cross, S. Ivanovski, D. Hutmacher, A. Pandit, D. Zeugolis, The influence of anisotropic nano- to micro-topography on in vitro and in vivo osteogenesis, Nanomedicine 10 (2015) 693–711, https://doi.org/10.2217/nnm.14.218.
[33] W. Chen, B. Tian, Y. Lei, Q.F. Ke, Z.A. Zhu, Y.P. Guo, Hydroxyapatite coatings with oriented nanoplate and nanorod arrays: fabrication, morphology, cytocompatibility and osteogenic differentiation, Mater. Sci. Eng. C 67 (2016) 395–408, https://doi.org/10.1016/j.msec.2016.04.106.
[34] S. Ramezani, R. Emadi, M. Kharaziha, F. Tavangarian, Synthesis, characterization and in vitro behavior of nanostructured diopside/biphasic calcium phosphate scaffolds, Mater. Chem. Phys. 186 (2017) 415–425, https://doi.org/10.1016/j.matchemphys.2016.11.013.
[35] H. Fleisch, S. Bisaz, Mechanism of calcification: inhibitory role of pyrophosphate, Nature 195 (1962), https://doi.org/10.1038/195911a0 undefined.
[36] N.A. Mata, P. Ros-Tárraga, P. Velasquez, A. Murciano, P.N. de Aza, Synthesis and characterization of 3D multilayer porous Si–Ca–P scaffolds doped with Sr ions to modulate in vitro bioactivity, Ceram. Int. 46 (2020) 968–977, https://doi.org/10.1016/j.ceramint.2019.09.058.
[37] E. Lamers, X. Frank Walboomers, M. Domanski, J. te Riet, F.C.M.J.M. van Delft, R. Luttge, L.A.J.A. Winnubst, H.J.G.E. Gardeniers, J.A. Jansen, The influence of nanoscale grooved substrates on osteoblast behavior and extracellular matrix deposition, Biomaterials 31 (2010) 3307–3316, https://doi.org/10.1016/j.biomaterials.2010.01.034.
[38] K. Anselme, P. Davidson, A.M. Popa, M. Giazzon, M. Liley, L. Ploux, The interaction of cells and bacteria with surfaces structured at the nanometre scale, Acta Biomater. 6 (2010) 3824–3846, https://doi.org/10.1016/j.actbio.2010.04.001.
[39] J.Y. Yang, Y.C. Ting, J.Y. Lai, H.L. Liu, H.W. Fang, W.B. Tsai, Quantitative analysis of osteoblast-like cells (MG63) morphology on nanogrooved substrata with various groove and ridge dimensions, J. Biomed. Mater. Res. 90 (2009) 629–640, https://doi.org/10.1002/jbm.a.32130.
[40] X. Lu, Y. Leng, Quantitative analysis of osteoblast behavior on microgrooved hydroxyapatite and titanium substrata, J. Biomed. Mater. Res. 66 (2003) 677–687, https://doi.org/10.1002/jbm.a.10022.
[41] S. Ber, G. Torun Köse, V. Hasirci, Bone tissue engineering on patterned collagen films: an in vitro study, Biomaterials 26 (2005) 1977–1986, https://doi.org/10.1016/j.biomaterials.2004.07.007.
[42] W.B. Tsai, Y.C. Ting, J.Y. Yang, J.Y. Lai, H.L. Liu, Fibronectin modulates the morphology of osteoblast-like cells (MG-63) on nano-grooved substrates, J. Mater. Sci. Mater. Med. 20 (2009) 1367–1378, https://doi.org/10.1007/s10856-008-3687-8.
[43] M. Vandrovcová, L. Bačáková, Adhesion, growth and differentiation of osteoblasts on surface-modified materials developed for bone implants, Physiol. Res. 60 (2011) 403–417, https://doi.org/10.33549/physiolres.932045.
[44] C. Chai, K.W. Leong, Biomaterials approach to expand and direct differentiation of stem cells, Mol. Ther. 15 (2007) 467–480, https://doi.org/10.1038/sj.mt.6300084.
[45] C. Zhao, X. Wang, L. Gao, L. Jing, Q. Zhou, J. Chang, The role of the micro-pattern and nano-topography of hydroxyapatite bioceramics on stimulating osteogenic differentiation of mesenchymal stem cells, Acta Biomater. 73 (2018) 509–521, https://doi.org/10.1016/j.actbio.2018.04.030.
[46] H.N. Kim, A. Jiao, N.S. Hwang, M.S. Kim, D.H. Kang, D.H. Kim, K.Y. Suh, Nanotopography-guided tissue engineering and regenerative medicine, Adv. Drug Deliv. Rev. 65 (2013) 536–558, https://doi.org/10.1016/j.addr.2012.07.014.
[47] E. Tamjid, A. Simchi, J.W.C. Dunlop, P. Fratzl, R. Bagheri, M. Vossoughi, Tissue growth into three-dimensional composite scaffolds with controlled micro-features and nanotopographical surfaces, J. Biomed. Mater. Res. A 101 (2013) 2796–2807, https://doi.org/10.1002/jbm.a.34584.